Compressibility Effects on High-Reynolds Coherent Structures via Two-Point Correlations

Christian J. Lagares-Nieves[1]* and Guillermo Araya[1]†
[1]*HPC and Visualization Lab, Dept. of Mechanical Eng., University of Puerto Rico at Mayaguez, PR 00681, USA.*

The importance of coherent structures in turbulent boundary layers has been extensively explored in the large corpora of available literature. Although their impact on heat, mass and passive/active scalar transport has been extensively documented, their dependency on the Mach number has not been widely explored. In the present work, we identify coherent structures based on two-point correlations of the fluctuating components of the quantities of interest. To efficiently compute these two-point correlations (TPC), we apply a low-memory, high-performance TPC implementation. The results for the streamwise velocity and temperature fluctuations are presented for an adiabatic flat plate at supersonic conditions at moderately high Reynolds numbers with friction Reynolds numbers, δ^+, in the order of 950. In the incompressible counterpart, the temperature is regarded as a passive scalar with isothermal wall condition. The results suggest weak compressibility effects at Mach 2.5 on both two-point correlations and their corresponding energy spectra. However, a slight breakdown of the Reynolds analogy is seen at Mach 2.5.

I. Nomenclature

U_i	=	Mean Velocity
P	=	Mean Pressure
T	=	Mean Temperature
k	=	Thermal conductivity
c_p	=	Specific heat at constant pressure
$\dot{q}$	=	Heat generation
M_∞	=	Freestream Mach Number
N_t	=	Number of Temporal Samples
N_s	=	Number of Additional Smoothing Samples
N_x	=	Number of Nodes Along the Streamwise Direction
N_y	=	Number of Nodes Along the Wall Normal Direction
N_z	=	Number of Nodes Along the Spanwise Direction
μ	=	Molecular Viscosity
ρ	=	Density
δ	=	Boundary layer thickness
δ^+	=	$\delta u_\tau / \nu_w$ Friction Reynolds number
u_τ	=	Friction velocity
ν_w	=	Wall kinematic viscosity
τ	=	Shear stress
κ	=	thermal conductivity
$'$	=	Superscript denotes fluctuating components
∞	=	Subscript denotes freestream quantities

*PhD Research Assistant & Doctoral Candidate, Department of Mechanical Engineering, 259 Alfonso Valdez Blvd., Mayaguez, PR, 00680, and Student Member
†Associate Professor, Department of Mechanical Engineering, 259 Alfonso Valdez Blvd., Mayaguez, PR, 00680. AIAA Associate Fellow

II. Introduction

Unsteady spatially-developing turbulent boundary layers (SDTBL) are of utmost importance to a wide range of disciplines and engineering applications, showing non-homogeneous conditions along the flow direction. Supersonic SDTBLs are ubiquitous and of crucial aspect to high speed flight conditions with applications ranging from space planes, to future commercial planes, military technologies, space exploration technologies, among many others. A key aspect of the understanding of SDTBLs is the description of coherent structures which play a crucial role in heat, momentum and passive/active scalar transport. Nonetheless, an inherent complexity in these coherent structures can be linked to the chaotic nature of turbulent flows. It has been argued that these complex patterns follow coherent dynamics where the level of coherence should be quantifiable [1]. Identifying these large (LSM) and very-large scales of motion (VLSM) can be done in a myriad of possible ways depending on how the problem is stated. One such avenue is to employ two-point correlations (TPC) [2] which can be efficiently computed with low memory requirements via high-performance inner products [3].

The nature and existence of these organized structures was explored early by Spina and Smits [4]. Rempfer and Fasel [5] also explored the nature of these coherent structures in a volumetric space. They employ proper orthogonal decomposition (POD) which translates the problem of computing these structures into an Eigenvalue problem. Closely related work by Aubry *et al.* [6], further reinforced the existence of a link between low-dimensional chaotic dynamics and properties of realistic turbulence. Smits *et al.* [7] also explored the structure of the turbulent boundary layer with a special focus on comparing the subsonic and supersonic SDTBLs. They concluded that albeit many similarities that were found, especially along the spanwise direction, there were drastic differences such as variations in length scales. The work by Ringuette *et al.*[8] explored volumetric coherent structures for a Mach 3 boundary layer and contrasted it with a subsonic boundary layer. Although they used several methods for visualizing said VLSMs, the two-point correlation was among the selected methodologies. Later work by Elsinga *et al.*[9] sought to explore the organization of vortex for high Reynolds supersonic SDTBLs. They also employed the autocorrelation function and provided conclusions related to the periodic nature of these coherent structures, their lengths and inclinations. More recently, TPC's have been employed to assess wall-temperature effects at hypersonic conditions [10] at low Reynolds numbers. Interestingly, wall cooling induced a transport direction change in the near wall region due to the local overheating of the boundary layer, which in turn caused intensification of ejections. Moreover, this ejection enhancement seemed to be the reason of the extremely long structures found in the buffer zone (at $y^+ \approx 15$, as seen in fig. 1) of hypersonic boundary layer subject to wall cooling. Although a large portion of work previously outlined has been computational in nature, work by He *et al.* [11] visualized these coherent structures for an experimental supersonic boundary layer over a flat plate. Another seminal contribution in incompressible flow was done by Sillero *et al.* [12] which was further elaborated by Jimenez [1] explored in detail the 3D nature of turbulent coherent structures by the two-point correlation. Sillero *et al.* [12] reports peak lengths for structures in the logarithmic and outer regions of 7 and 18 δ. Furthermore, they highlight that structures at and below the buffer region are similar between channel and wall-bounded flow. Dharmarathne *et al.* provided a more applied view of the impact of turbulent coherent structures in passive scalar transport [13] via DNS of incompressible channel flows and TPC. It was stated that the LSMs which transport streamwise component of the turbulence kinetic energy, passive scalar variance, and streamwise heat flux are evidently different to each other beyond the buffer region.

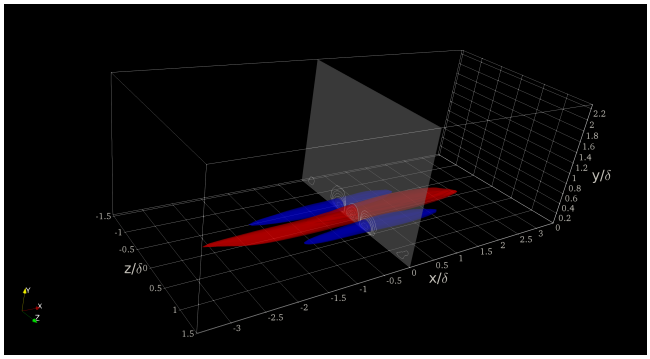

Fig. 1 Wall cooling effect on momentum turbulent structures at $y^+ = 15$ via TPC of streamwise velocity fluctuations.

In the present work, we conduct a study of the compressibility effects on TPCs for an SDTBL subject to Zero Pressure Gradient (ZPG) (i.e., flat plate) via DNS. The results will shed light on the impact of supersonic conditions on the homogeneity of the flow and the momentum/thermal transport characteristics. We compare a ZPG, adiabatic flat plate at Mach 2.5 at moderately high Reynolds numbers with an "incompressible companion". In the incompressible regime, temperature is regarded as a passive scalar and isothermal wall conditions. In summary, the only variable parameter is the Mach number.

III. Governing Equations

Assuming continuum mechanics and neglecting non-equilibrium effects yields the usual system of non-linear partial differential equations known as the compressible Navier-Stokes equations [14]. Conservation of mass becomes non-trivial for compressible flow with strong pressure gradients, compression and expansion waves where density varies abruptly. The classical conservation equations are presented in eqns. 1, 2 and 3.

$$\frac{\partial \rho}{\partial t} + \frac{\partial}{\partial x_j}\left(\rho u_j\right) = 0 \tag{1}$$

$$\frac{\partial \rho u_i}{\partial t} + \frac{\partial}{\partial x_j}\left(\rho u_i u_j + p\delta_{ij} - \sigma_{ij}\right) = 0 \tag{2}$$

$$\frac{\partial \rho e}{\partial t} + \frac{\partial}{\partial x_j}\left((\rho e)u_j - u_i\sigma_{ij} + q_j\right) = 0 \tag{3}$$

where ρ is the density; u_i is the velocity in the i direction; p is the pressure; σ_{ij} is the stress tensor which we model as a linear stress-strain relationship,

$$\sigma_{ij} = 2\mu S_{ij} - \frac{2}{3}\mu\delta_{ij}S_k k \tag{4}$$

where $S_{ij} = \frac{1}{2}\left(\frac{\partial u_i}{\partial x_j} + \frac{\partial u_j}{\partial x_i}\right)$ is the strain rate tensor, μ is the kinematic viscosity; and q_i is the hear flux due to thermal gradients in the i direction and is modelled in the present work by Fourier's law, $q_i = \kappa\frac{\partial T}{\partial x_i}$ where κ is the thermal conductivity; e is total energy per unit mass which we assume to follow:

$$e = c_v T + \frac{1}{2}u_i u_j \tag{5}$$

where c_v is the specific heat at constant volume. Finally, we also assume the fluid viscosity to vary following a Power Law (see Equation 6).

$$\mu = \mu_\infty\left(\frac{T}{T_\infty}\right)^{0.76} \tag{6}$$

The equations are all presented in their strong form whereas the weak form is used in the finite element solver. The present work leverages the PHASTA flow solver [15]. The finite element scheme is based on the streamline upwind Petrov-Galerkin (SUPG) finite element discretization in space with a second order accuracy [16, 17]. The non-linear system of equations are solved using an iterative Krylov solver in space while being fully implicit in time (2^{nd} order accurate). Further details regarding the finite element method employed are beyond the scope of this work, readers are referred to [18].

IV. Numerical Details

A. DNS Details

Modeling effort of the physics of turbulent spatially-developing boundary layers by using DNS must tackle the following aspects: (a) the mesh resolution must be adequate in order to capture the smallest turbulence momentum/thermal scales (Kolmogorov and Batchelor scales), (b) the computational box must be sufficiently large to "gather" the influence of the turbulent large scale motions (LSM) or "superstructures" (Hutchins & Marusic [19]), (c) realistic time-dependent inflow turbulent fluctuations must be injected, Araya *et al.*, [20] [21]. A key aspect on the simulations of unsteady turbulent boundary layers that evolve in space is the prescription of accurate turbulent inflow information. In the present article, the inlet generation methodology proposed by Araya *et al.* [20] is utilized, called Dynamic Multiscale Approach (DMA). It is a modified version of the rescaling-recycling technique by Lund *et al.* [22]. Extensions to compressible boundary layers have also been proposed by Urbin & Knight [23], Stolz & Adams [24] and Xu & Martin [25]. A block diagram is shown in fig. 2. The seminal idea of the rescaling-recycling method is to extract the flow solution (mean and fluctuating components of the velocity, thermal and pressure fields for compressible flows) from a downstream plane (called "recycle") and after performing a transformation by means of scaling functions, the transformed profiles are re-injected at the inlet plane, as seen in figure 2. In fact, it has been observed in compressible boundary layers that just

fixing the mean pressure at the inlet produced more stable and accurate numerical cases that adding pressure fluctuations. According to [26] and [23], "the static pressure can be assumed constant at the inlet plane since the pressure fluctuations are small compared to the static temperature fluctuations". Instantaneous density profiles (mean plus fluctuations) are indirectly imposed due to the equation of state for a perfect gas via instantaneous temperature profiles. The main purpose of implementing scaling laws to the flow solution is to convert the streamwise in-homogeneity of the flow into quasi-homogeneous conditions. The Reynolds decomposition is implemented for instantaneous parameters, i.e. a time-averaged plus a fluctuating component:

$$u_i(\mathbf{x}, t) = U_i(x, y) + u_i'(\mathbf{x}, t) \tag{7}$$

$$t(\mathbf{x}, t) = T(x, y) + t'(\mathbf{x}, t) \tag{8}$$

The turbulent boundary layer is divided into inner and outer zones, where different scaling laws are applied [20] in a multiscale fashion. The projection of flow parameters from the recycle plane to the inlet is performed along constant values of y^+ (inner region) and y/δ (outer region). Figure 2 depicts the schematic of the computational domain in the incompressible regime and at high Reynolds numbers. In the re-scaling process of the flow parameters [20], the ratio of the inlet friction velocity to the recycle friction velocity (i.e., $\lambda = u_{\tau,inl}/u_{\tau,rec}$) is required. The friction velocity is defined as $u_\tau = \sqrt{\tau_w/\rho}$, where τ_w is the wall shear stress and ρ is the fluid density. Since the inlet boundary layer thickness must be prescribed according to the predicted inlet Reynolds number, prescribing also the inlet friction velocity would be redundant. To overcome this problem, Lund *et al.* [22], Urbin & Knight [23] and Stolz & Adams [24] employed the well-known 1/8-power law that relates the friction velocity to the momentum thickness in zero-pressure gradient flows; thus, $u_{\tau,inl}/u_{\tau,rec} = (\delta_{2,inl}/\delta_{2,rec})^{-1/8}$. The empirical power (-1/8) is strongly affected by the Reynolds number dependency plus some compressibility effects; therefore, we "dynamically" calculate this power exponent, $\gamma_{\delta 2}$, by relating the mean flow solution from a new plane (so-called the "Test" plane, as seen in figure 2) to the solution from the recycle plane as follows:

$$\gamma_{\delta 2} = \frac{ln(u_{\tau,test}/u_{\tau,rec})}{ln(\delta_{2,test}/\delta_{2,rec})}. \tag{9}$$

Figure 3 (a) exhibits a representative time series of the computed friction velocities at the Inlet, Test and Recycle planes in the supersonic flat plate at high Reynolds numbers. Friction velocity has been normalized by the local freestream velocity. This supersonic case was initialized via the incompressible DNS case. It is observed a clear transient stage ($t^+ \approx 4000$) where friction velocities fluctuate wildly. Beyond $t^+ \approx 4000$, all friction velocities tend asymptotically towards specific values. Friction velocities at the test and recycle plane (as well as momentum thicknesses) are computed "on the fly" based on the time-averaged parameters from the flow solution. Once the exponent $\gamma_{\delta 2}$ is obtained from Eq. 9 based on test and recycle plane statistics, the values of $u_{\tau,inl}$ and λ can be calculated. As can be observed in fig. 3 (b), the $\lambda = u_{\tau,inl}/u_{\tau,rec}$ parameter approaches a value of 1.022 in the statistically steady stage.

In order to perform the proposed DNS at high Reynolds numbers, a highly accurate, very efficient, and highly scalable CFD solver is required. The flow solver PHASTA is an open-source, parallel, hierarchic (2^{nd} to 5^{th} order accurate), adaptive, stabilized (finite-element) transient analysis tool for the solution of compressible [18] or incompressible flows [16]. PHASTA has been extensively validated in a suite of DNS under different external conditions [10, 27, 28].

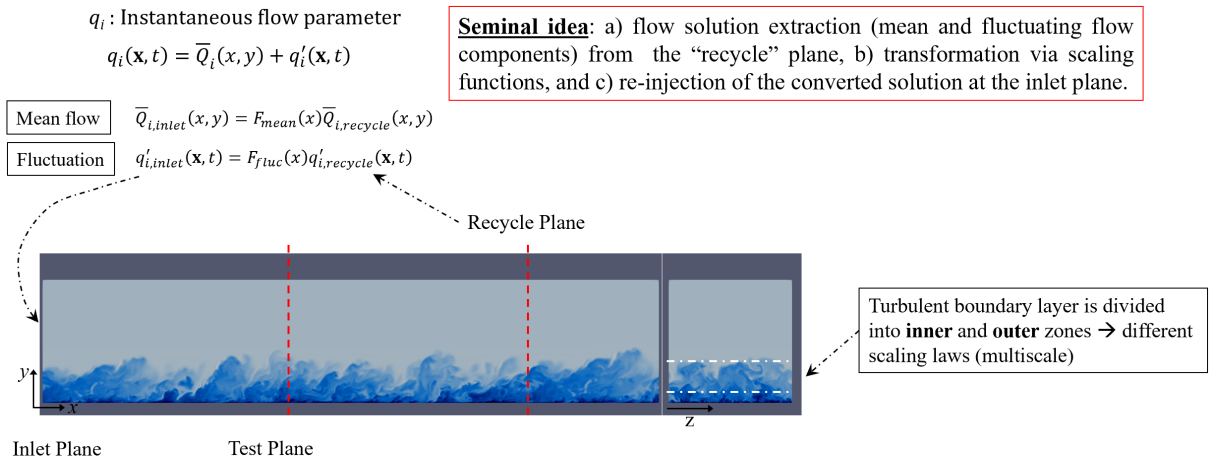

Fig. 2 The Dynamic Multiscale Approach (DMA).

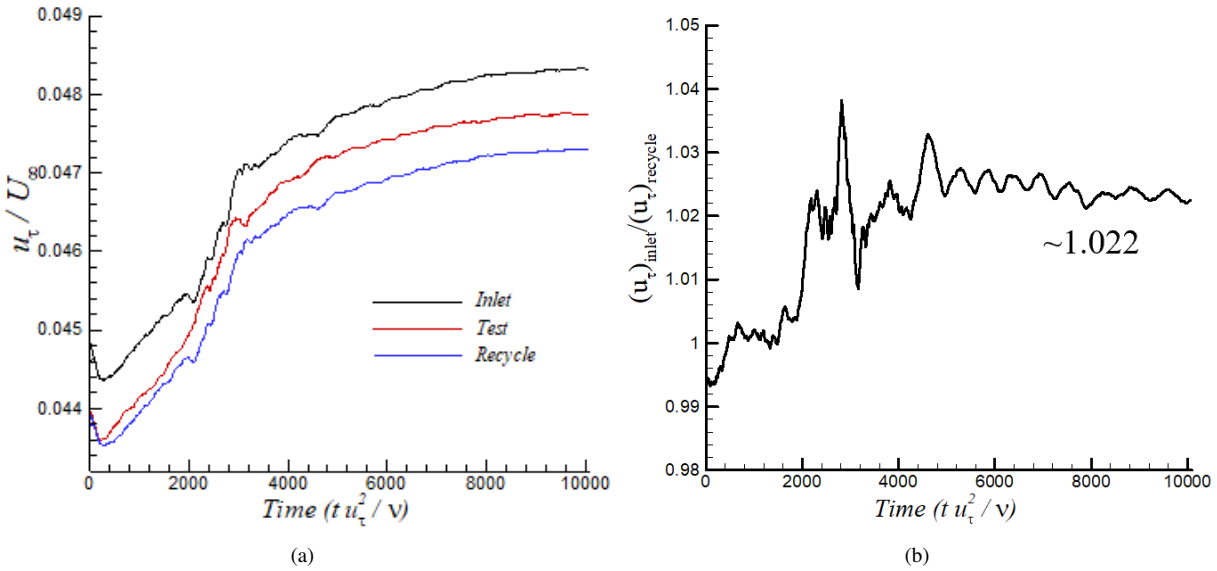

(a) (b)

Fig. 3 (a) Time-series of the friction velocity normalized by the local freestream velocity and (b) friction velocity ratio variation for supersonic flow and adiabatic wall condition.

Boundary Conditions: At the wall, the classical no-slip condition is imposed for all velocity components. Quasi-adiabatic wall condition is assumed for the thermal field in the compressible flow case, the ratio T_w/T_∞ is 2.25, where T_w is the wall temperature and T_∞ is the freestream temperature. The T_r/T_∞ ratio is 2.12 for M_∞ equals to 2.5; therefore, $T_w/T_r \approx 1.06$. T_r is the recovery or adiabatic temperature. In the incompressible case, temperature is regarded as a passive scalar, in both cases the Prandtl number is 0.72. The lateral boundary conditions are handled via periodicity; whereas, freestream values are prescribed on the top surface.

Table 1 summarizes the characteristics of the analyzed two cases: the incompressible case ($M_\infty = 0$) and compressible case ($M_\infty = 2.5$). The Reynolds number range, computational domain dimensions in terms of the inlet boundary layer thickness δ_{inl} (where L_x, L_y and L_z represent the streamwise, wall-normal and spanwise domain length, respectively) and mesh resolution in wall units (Δx^+, Δy^+_{min}, Δy^+_{max}, Δz^+) are also given. The DNS cases have the following grid point number: $990 \times 250 \times 210$ (roughly a 52-million point mesh). The cases were run in 1200 processors at the Blue Waters supercomputer (NCSA) and Onyx (DoD).
Figure 4 (a) shows the streamwise development of the skin friction coefficient of present DNS supersonic data at high

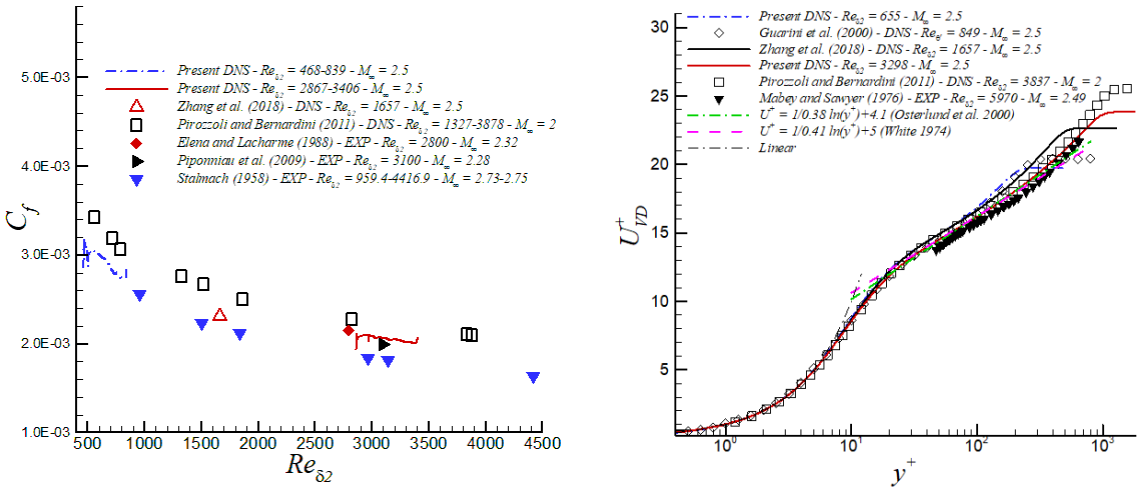

(a) (b)

Fig. 4 (a) Skin friction coefficient and (b) mean streamwise velocity in wall units.

Reynolds numbers. In addition, C_f values are included at low Reynolds numbers from our group [21]. It is important to note the excellent agreement of present DNS with experiments at similar conditions, i.e. experimental data from [29] and [30]. For the time-averaged streamwise velocity in wall units and compressible flow, the van Driest transform is applied. In Figure 4 (b), it is seen a good agreement of present DNS data at Mach 2.5 and experimental data from Mabey and Sawyer [31] at slightly higher Reynolds numbers and Mach 2.29. Furthermore, our DNS data exhibits an excellent collapse with DNS from Pirozzoli and Bernardini [32] at very similar Reynolds numbers and Mach 2. This may indicate that compressibility effect is weak under these supersonic conditions, and the van Driest transform is able to absorb it. The log region is very large in our DNS profile at $Re_{\delta 2} = 3298$, extending roughly 280 wall units. Log coefficients proposed by Osterlund *et al.* [33] and White [34] describe quite well the logarithmic behavior.

Table 1 DNS Cases.

Case	M_∞	$Re_{\delta 2}$	$L_x \times L_y \times L_z$	Δx^+,$\Delta y^+_{min}/\Delta y^+_{max}$, Δz^+
Incompressible	0	2000-2400	$16\delta_{inl} \times 3\delta_{inl} \times 3\delta_{inl}$	11.5, 0.4/10, 10
Supersonic	2.5	2867-3406	$15.1\delta_{inl} \times 3\delta_{inl} \times 3\delta_{inl}$	11.9, 0.4/11, 11

B. High-Performance, Low-Memory Two-Point Correlation

The two-point correlations presented in this work were calculated leveraging the in-house, out-of-core, distributed library Aquila [3]. Aquila operates on larger-than-memory datasets efficiently via a high-performance data pre-fetcher capable of providing the illusion of an in-memory dataset. This is crucial given the limited amount of memory in modern supercomputing node architectures. Full domain two-point correlation has $O(N_t * N_s * N_x * N_y * N_z^2)$ operations per correlation. Although operating in the Fourier domain via the Convolution Theorem [35–37] would reduce the spanwise quadratic dependency to a logarithmic dependency, it doubles the memory requirement which, as was previously alluded, is a limiting factor. Thus, Aquila implements a highly efficient TPC atop dot products. For x86-64, Aquila leverages AVX instructions for a small vector dot product which provides higher performance than Intel's Math Kernel Library; nonetheless, Aquila is portable across architectures with general backends due to its use of Kokkos [38].
We formulate the two-point correlation as,

$$R_{kk}(\mathbf{x};\mathbf{r}) = \frac{1}{N_t}\frac{1}{N_s}\sum_{t=1}^{N_t}\sum_{s=1}^{N_s}\langle k'(t,\mathbf{x}+\mathbf{x_s}), k'(t,\mathbf{x}+\mathbf{x_s}+\mathbf{r})\rangle \tag{10}$$

where k is representative of a flow variable and $\mathbf{r}$ is the offset (or lag) from a given reference point, $\mathbf{x}$. Thus, $O(N_t * N_s)$ dot products are executed per domain node. We sample all spanwise nodes due to the homogeneity along the spanwise direction due to the periodic boundary conditions imposed, and we also considered a total of 80 stations ($\mathbf{x_s}$) along the streamwise location. This provides additional information and smooths out noise inherent in the statistical samples made. Further details about the design and implementation of Aquila can be found in [3] and are outside the scope of this paper. However, we present evidence of Aquila's strong scaling in fig. 5 for a Cray XC40/50 using Intel Broadwell CPUs, Onyx. As seen from the figure, Aquila is capable of scaling out to over 100,000 CPU cores with a parallel efficiency above 80% and with >95% parallel efficiency to just over 50,000 cores. The loss of parallel efficiency is likely due to a saturation of network resources once 50% of the available compute nodes are being used. A more recent version of Aquila was used for the calculation of the energy spectra. This recent version of Aquila leverages FFTs in multiple calculations including TPCs and energy spectra. The energy spectra use MKL's FFTW in single precision mode.

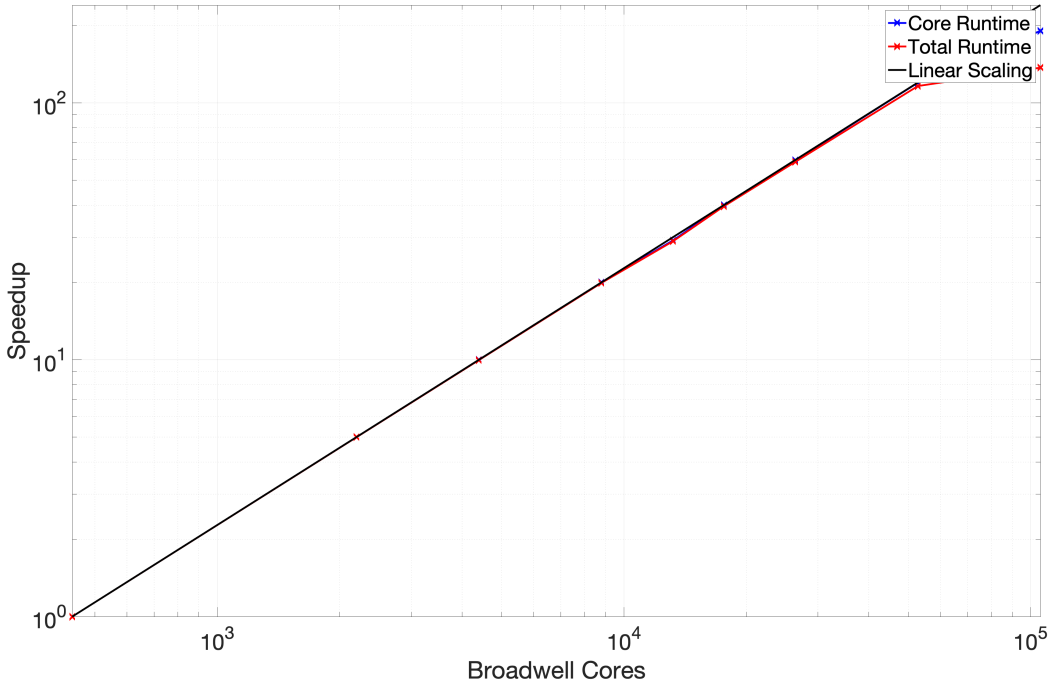

Fig. 5 Aquila's Post-Processing Strong Scaling Performance [3]

V. Results and Discussion

A. Two-Point Correlations

The present study focuses on compressibility effects on velocity and thermal two-point correlations in the buffer region. The buffer region was chosen due to the presence of high mean velocity gradients and strong turbulence nature. This region is characterized by highly energetic small, length-scales and peak transfer rates of energy from the mean-flow to the turbulent kinetic energy. Furthermore, the supersonic effects on the Reynolds analogy are inferred by comparing velocity and thermal structures.

The time-averaged two-point correlations are compared along the streamwise and wall-normal axis in fig 6. Incompressible and supersonic streamwise velocity fluctuations depict a strong correlation with downstream parcels of fluid, showing upstream "tails" in the order of 1δ. Notice that a slightly thicker structure is observed in the incompressible regime. The contrary is true for the thermal structures that experience a significant vertical thickening at Mach 2.5. The Reynolds analogy approximately holds for incompressible flow in the buffer region (y^+ = 15); however some differences between momentum and thermal structures are noticeable in the supersonic case. In fig. 7 isometric views of R_{tt} can be observed.

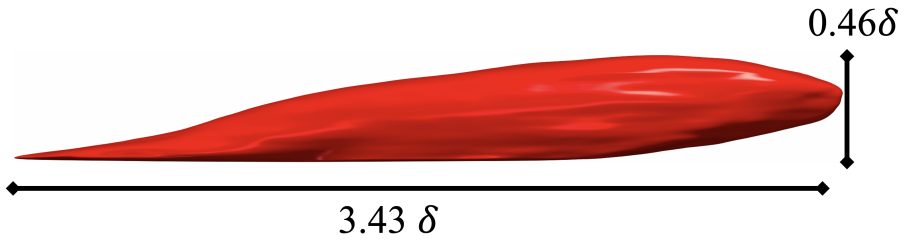

(a) Incompressible

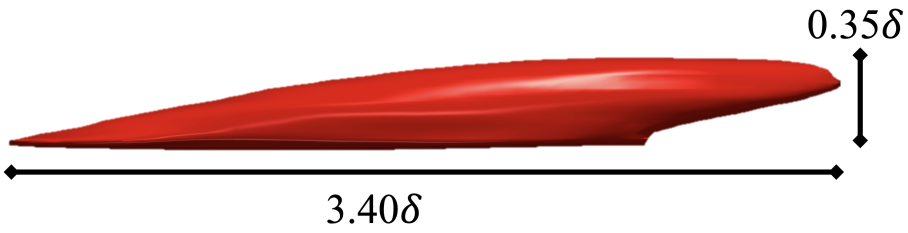

(b) Supersonic

Fig. 6 3D Two-Point Correlation of streamwise velocity fluctuations (R_{uu}) at $y^+ = 15$. Both structures measure roughly 0.33 δ in the spanwise direction.

In this case, a threshold of 15% of the maximum value of R_{tt} was extracted. Again, thermal fluctuations exhibit a clear tendency to vertically "grow" in the supersonic regime. The Reynolds analogy is evaluated by analyzing the cross-correlation between streamwise velocity fluctuations u' and thermal fluctuations t', i.e. R_{ut}. Both parameters depict a high level of correlation, with streamwise lengths in the order of 2.5δ, being δ the local momentum boundary layer thickness. Interestingly, the similarity between iso-surfaces of R_{ut} in the incompressible and supersonic regime is impressive, indicating that the Reynolds analogy possesses a weak effect of the Mach number (compressibility), at least for the conditions (Reynolds number and wall adiabatic conditions) considered in our DNS approach. Let's recall that the temperature in the incompressible case was assumed a passive scalar with isothermal conditions.

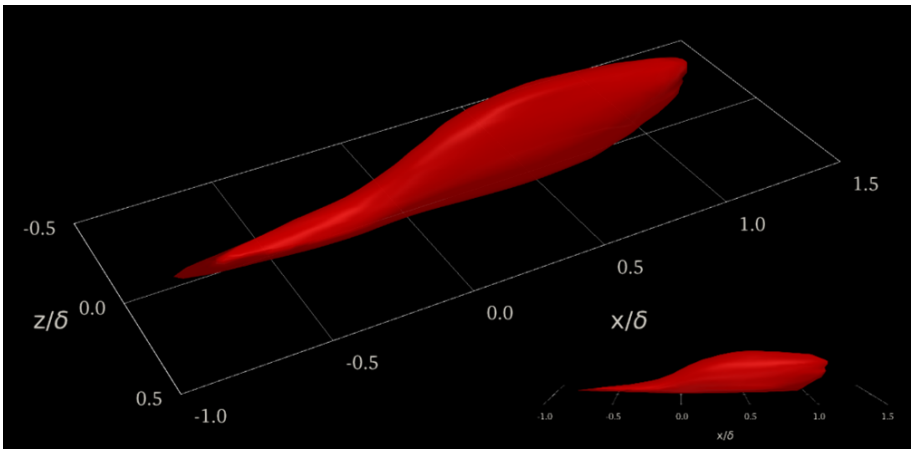

(a) Incompressible

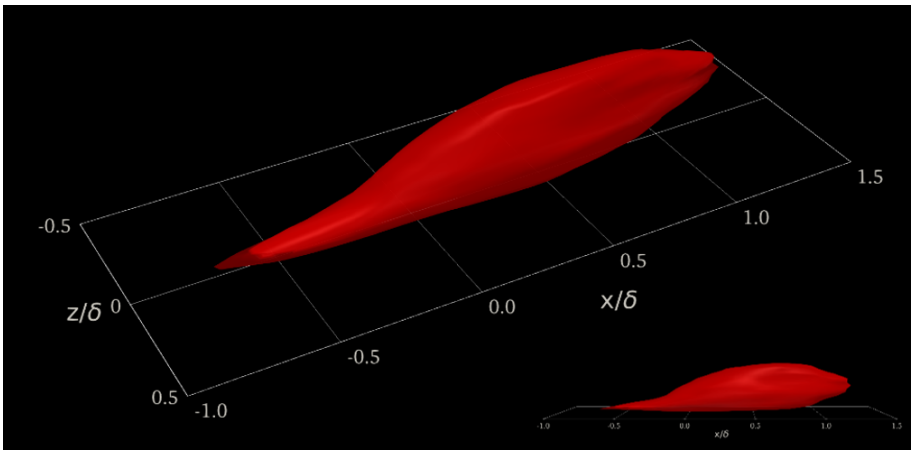

(b) Supersonic

Fig. 7 3D Two-Point Correlation of thermal fluctuations (R_{tt}) at $y^+ = 15$.

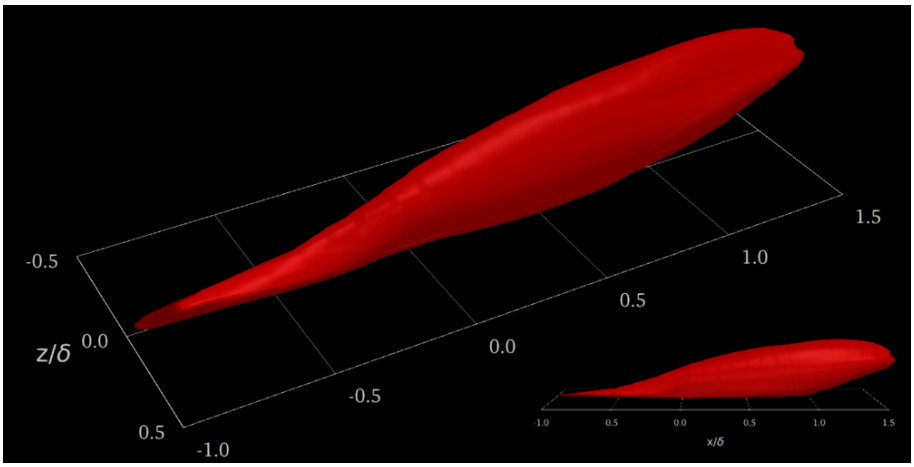

(a) Incompressible

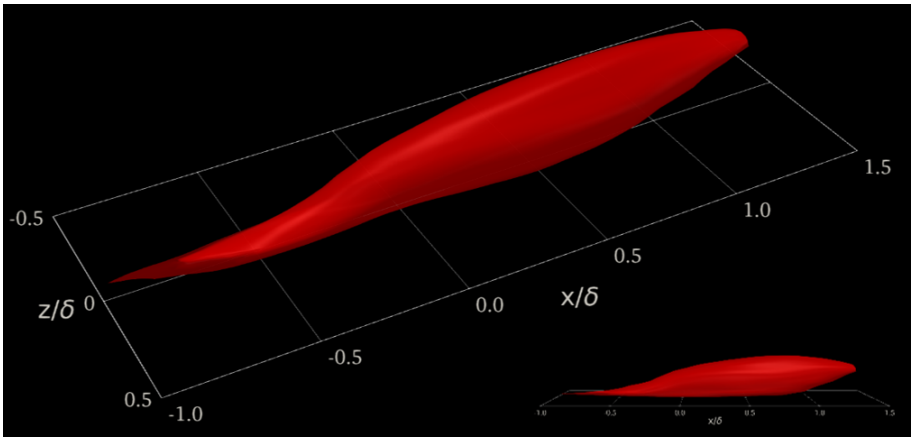

(b) Supersonic

Fig. 8 3D Two-Point Cross-correlations of $u't'$ (R_{ut}) at $y^+ = 15$.

B. Energy Spectra

The energy spectra was computed as the magnitude of the Fourier transform of the spanwise TPC. The normalized energy spectra are presented in Figure 9. The normalization was chosen to facilitate a comparison between the incompressible and supersonic conditions. The inertial subrange's slope (i.e., -5/3) agrees with the expected theoretical one. What is more notable is the extension of the dissipation range and its high degree of agreement with the theoretical value of -3 associated to enstrophy transfer. In fact, a power law can be fitted to the dissipation range in all cases with an $R^2 \geq 0.97$. Furthermore, the inflection point towards the end of the dissipation range serves as an indication that the Kolmogorov scales are being accurately captured.

What is more, compressibility effects in the energy cascade are relatively weak. Perhaps the most notable effect is the slightly more compressed spectra under supersonic conditions which is consistent across both the velocity and temperature spectra. Particularly, the energetic level of turbulent eddies is slightly lower in the inertial subrange (and for lower waivenumbers) for the supersonic regime. However, both are qualitatively similar.

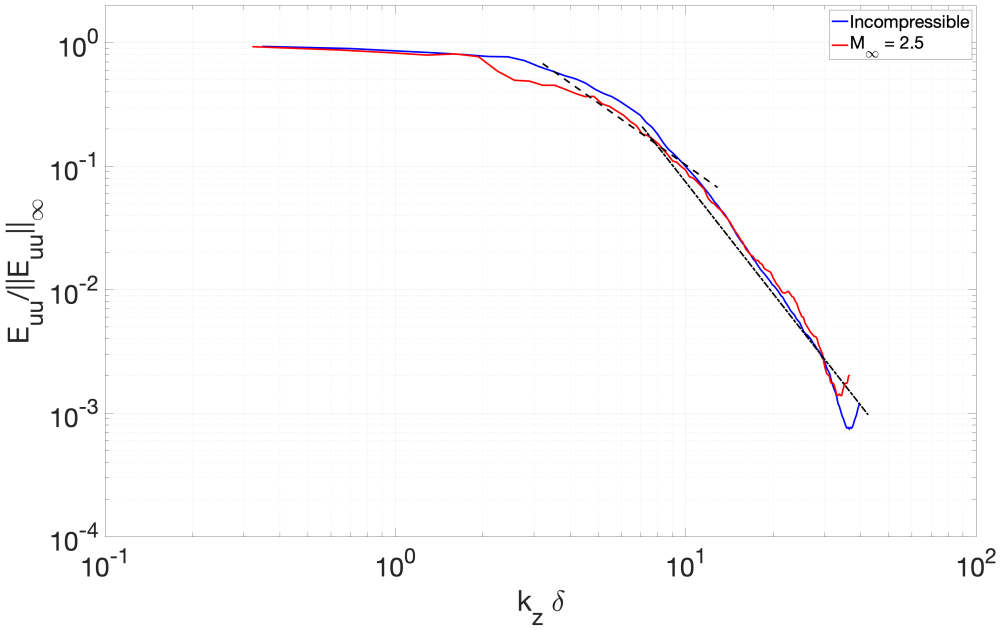

(a) Streamwise Velocity Energy Spectra

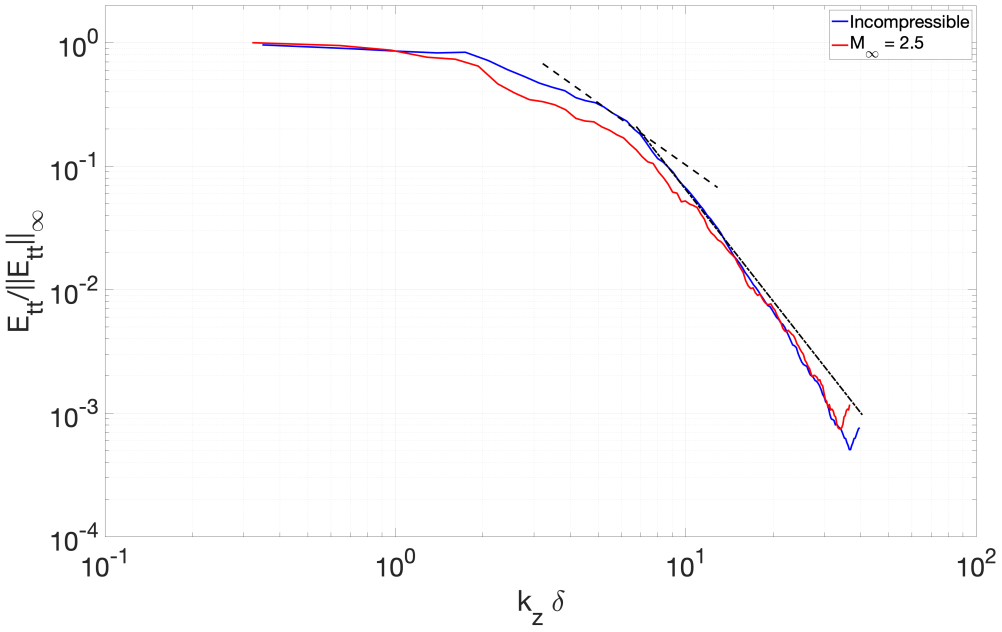

(b) Temperature Energy Spectra

Fig. 9 Normalized spanwise energy spectra at $y^+ = 15$; the dashed line (- - - - - - -) corresponds to a power law with exponent $-5/3$; the dash-dot line (-·-·-·-·-) corresponds to a power law with exponent -3.

VI. Future Work

The present work currently shows results in the buffer region. In the future, we plan to include results in the viscous sublayer and the outer layer. As a starting point, we aimed at the buffer layer due to the key phenomena occurring in this region. Furthermore, we are conducting larger sampling studies to account for larger portions that are

quasi-homogeneous in the streamwise direction. This should result in smoother, more defined structures and a reduction in the amount of noise present in the energy spectra.

VII. Conclusion

Compressibility effects on turbulent boundary layers subject to zero-pressure gradients at moderately high Reynolds numbers were explored via two-point correlations. The two-point correlations were computed in the physical domain using a low-memory, high-performance implementation in Aquila, an in-house post-processing library. The presented structures suggest weak compressibility effects with a slight weakening of the Reynolds analogy observed at supersonic conditions; nonetheless, the variations are slight. The energy spectra also suffers weak compressibility effects. What is more, both the velocity and temperature fluctuation spectra agree to a significant degree with the classical theoretical slopes.

Acknowledgments

This material is based upon work supported by the National Science Foundation under Grant No. HRD-1906130 and Grant No. 1847241. This work was supported in part by a grant from the Air Force Office of Scientific Research (grant no. FA9550-17-1-0051). This work was supported in part by a grant from the DoD High-Performance Computing Modernization Program (HPCMP).

References

[1] Jimenéz, J., "Coherent structures in wall-bounded turbulence," *Journal of Fluid Mechanics*, Vol. 842, 2018, p. 842.

[2] Pope, S. B., *Turbulent Flows*, Cambridge University Press, 2000.

[3] Lagares, C., Rivera, W., and Araya, G., "Aquila: A Distributed and Portable Post-Processing Library for Large-Scale Computational Fluid Dynamics," *AIAA SciTech*, 2021.

[4] Spina, E. F., and Smits, A. J., "Organized structures in a compressible, turbulent boundary layer," *Journal of Fluid Mechanics*, Vol. 182, 1987, pp. 85–109.

[5] Rempfer, D., and Fasel, H. F., "Dynamics of three-dimensional coherent structures in a flat-plate boundary layer," *Journal of Fluid Mechanics*, Vol. 275, 1994, pp. 257–283.

[6] Aubry, N., Holmes, P., Lumley, J. L., and Stone, E., "The dynamics of coherent structures in the wall region of a turbulent boundary layer," *Journal of Fluid Mechanics*, Vol. 192, 1988, pp. 115–173.

[7] Smits, A. J., Spina, E. F., Alving, A. E., Smith, R. W., Fernando, E. M., and Donovan, J. F., "A comparison of the turbulence structure of subsonic and supersonic boundary layers," *Physics of Fluids*, Vol. 1, No. 11, 1989, pp. 1865–1875.

[8] Ringuette, M. J., Wu, M., and Martin, M. P., "Coherent structures in direct numerical simulation of turbulent boundary layers at Mach 3," *Journal of Fluid Mechanics*, Vol. 594, 2008, pp. 59–69.

[9] Elsinga, G. E., Adrian, R. J., van Oudheusden, B. W., and Scarano, F., "Three-dimensional vortex organization in a high-Reynolds-number supersonic turbulent boundary layer," *Journal of Fluid Mechanics*, Vol. 644, 2010, pp. 35–60.

[10] Araya, G., Lagares, C., Santiago, J., and Jansen, K., "Wall temperature effect on hypersonic turbulent boundary layers via DNS," *AIAA Scitech 2021 Forum (AIAA-2021-1745)*, 2021. https://doi.org/10.2514/6.2021-1745.

[11] He, L., ShiHe, Y., YuXin, Z., LiFeng, T., and Zhi, C., "Visualization of Coherent Structures in a Supersonic Flat-Plate Boundary Layer," *Chinese Science Bulletin*, Vol. 56, No. 6, 2011, pp. 489–494.

[12] Sillero, J., Jimenez, J., and Moser, R., "Two-point statistics for turbulent boundary layers and channels at Reynolds numbers up to $\delta^+ \approx 2000$," *Physics of Fluids*, Vol. 26, No. 10, 2014, 105109.

[13] Dharmarathne, S., Tutkun, M., Araya, G., and Castillo, L., "Structures of scalar transport in a turbulent channel," *European Journal of Mechanics B-Fluids*, Vol. 55, No. 2, 2016, pp. 259–271.

[14] Martin, M. P., "Direct numerical simulation of hypersonic turbulent boundary layers. Part 1. Initialization and comparison with experiments," *Journal of Fluid Mechanics*, Vol. 570, 2007, pp. 347–364.

[15] Jansen, K., "Unstructured grid large eddy simulation of wall bounded flow," *Annual Research Briefs*, Center for Turbulence Research, NASA Ames / Stanford University, 1993, pp. 151–156.

[16] Jansen, K. E., "A stabilized finite element method for computing turbulence," *Comp. Meth. Appl. Mech. Engng.*, Vol. 174, 1999, pp. 299–317.

[17] Jansen, K. E., Whiting, C. H., and Hulbert, G. M., "A generalized-α method for integrating the filtered Navier-Stokes equations with a stabilized finite element method," *Comp. Meth. Appl. Mech. Engng.*, Vol. 190, 1999, pp. 305–319.

[18] Whiting, C. H., Jansen, K. E., and Dey, S., "Hierarchical basis in stabilized finite element methods for compressible flows," *Comp. Meth. Appl. Mech. Engng.*, Vol. 192, No. 47-48, 2003, pp. 5167–5185.

[19] Hutchins, N., and Marusic, I., "Evidence of very long meandering features in the logarithmic region of turbulent boundary layers," *Journal of Fluid Mechanics*, Vol. 579, 2007, pp. 1–28.

[20] Araya, G., Castillo, L., Meneveau, C., and Jansen, K., " A dynamic multi-scale approach for turbulent inflow boundary conditions in spatially evolving flows," *Journal of Fluid Mechanics*, Vol. 670, 2011, pp. 518–605.

[21] Araya, G., Lagares, C., and Jansen, K., "Reynolds number dependency in supersonic spatially-developing turbulent boundary layers," *2020 AIAA SciTech Forum (AIAA 3247313) 6 - 10 January, Orlando, FL.*, 2020.

[22] Lund, T., Wu, X., and Squires, K., "Generation of turbulent inflow data for spatially-developing boundary layer simulations," *Journal of Computational Physics*, Vol. 140, No. 2, 1998, pp. 233–258.

[23] Urbin, G. and Knight, D., "Large-Eddy Simulation of a supersonic boundary layer using an unstructured grid," *AIAA Journal*, Vol. 39, No. 7, 2001, pp. 1288–1295.

[24] Stolz, S., and Adams, N., "Large-eddy simulation of high-Reynolds-number supersonic boundary layers using the approximate deconvolution model and a rescaling and recycling technique," *Physics of Fluids*, Vol. 15, No. 8, 2003, pp. 2398–2412.

[25] Xu, S., and Martin, M. P., "Assessment of inflow boundary conditions for compressible turbulent boundary layers," *Physics of Fluids*, Vol. 16, No. 7, 2004, pp. 2623–2639.

[26] Kistler, A., and Chen, W., "A Fluctuating Pressure Field in a Supersonic Turbulent Boundary Layer," *Journal of Fluid Mechanics*, Vol. 16, 1963, pp. 41–64.

[27] Araya, G., Castillo, C., and Hussain, F., "The log behaviour of the Reynolds shear stress in accelerating turbulent boundary layers," *Journal of Fluid Mechanics*, Vol. 775, 2015, pp. 189–200.

[28] Doosttalab, A., Araya, G., Newman, J., Adrian, R., Jansen, K., and Castillo, L., "Effect of small roughness elements on thermal statistics of a turbulent boundary layer at moderate Reynolds number," *Journal of Fluid Mechanics*, Vol. 787, 2015, pp. 84–115.

[29] Piponniau, S., Dussauge, J., Debieve, J. F., and Dupont, P., "A simple model for low-frequency unsteadiness in shock-induced separation," *Journal of Fluid Mechanics*, Vol. 629, 2009, pp. 87–108.

[30] Elena, M., and Lacharme, J., "Experimental study of a supersonic turbulent boundary layer using a laser doppler anemometer," *J. of Mec. Theor. Appl.*, Vol. 7, 1988, pp. 175–190.

[31] Mabey, D. and Sawyer, W., "Experimental Studies of the Boundary Layer on a Flat Plate at Mach Numbers from 2.5 to 4.5," *Aerodynamics Department, R.A.E., Bedford.*, Vol. Reports and Memoranda No. 3784, 1976.

[32] Pirozzoli, S., and Bernardini, M., "Turbulence in supersonic boundary layers at moderate Reynolds number," *Journal of Fluid Mechanics*, Vol. 688, 2011, pp. 120–168.

[33] Osterlund, J. and Johansson, A. and Nagib, H. and Hites, M., "A note on the overlap region in turbulent boundary layers," *Phys. Fluids*, Vol. 12, 2000, p. 1.

[34] White, F. M., *Viscous Fluid Flow*, McGraw-Hill Mechanical Engineering, New York, 2006.

[35] Arfken, G., *Mathematical Methods for Physicists*, Academic Press, 1985.

[36] Bracewell, R., *The Fourier Transform and Its Applications*, New York: McGraw-Hill, 1999.

[37] Box, G. E. P., Jenkins, G. M., Reinsel, G. C., and Ljung, G. M., *Time Series Analysis: Forecasting and Control*, 2015.

[38] Edwards, H. C., Trott, C. R., and Sunderland, D., "Kokkos: Enabling manycore performance portability through polymorphic memory access patterns," *Journal of Parallel and Distributed Computing*, Vol. 74, No. 12, 2014, pp. 3202–3216. https://doi.org/10.1016/j.jpdc.2014.07.003.